ADVANCED MATERIALS
www.advmat.de

Direct Observation of Oxygen Atoms Taking Tetrahedral Interstitial Sites in Medium-Entropy Body-Centered-Cubic Solutions

Chang Liu, Jizhe Cui, Zhiying Cheng, Bozhao Zhang, Siyuan Zhang, Jun Ding, Rong Yu, and En Ma**

Interstitial solutes, such as carbon in steels, are effective solid-solution hardening agents. These alloying elements are believed to occupy the octahedral interstices in body-centered-cubic (bcc) metals. Using deep-sub-angstrom-resolution electron ptychography, here the first experimental evidence to directly observe individual oxygen atoms in a highly concentrated bcc solid solution—the $(TiNbZr)_{86}O_{12}C_1N_1$ medium-entropy alloy (MEA)—is provided, whereby the interstitial sites in which the oxygen atoms are located are discerned. In addition to oxygen interstitials residing in octahedral sites, the first unambiguous evidence of a switch in preference to the unusual tetrahedral sites at high oxygen concentrations is shown. This shift away from octahedral occupancy is explained as resulting from the extra cost of strain energy when the requisite displacement of the host atoms is deterred in the presence of nearby octahedral interstitials.

1. Introduction

Interstitial solutes such as oxygen, carbon, and nitrogen are highly effective in providing solid solution strengthening in body-centered-cubic (bcc) metals.[1] A solute concentration of only a few hundred ppm can raise the yield strength of the bcc host by ≈100 MPa at room temperature, the popular steel (carbon in iron) being an example in this regard.[2] This effectiveness, of course, has to do with the location of carbon atoms inside the iron crystal; they reside in octahedral interstices in the bcc lattice to produce asymmetric local strains to effectively interact with and hold off the moving dislocations.[3] Each bcc unit cell contains 6 octahedral (O) interstitial sites and 12 tetrahedral (T) interstitial sites, with the radius (r) of the T-site being approximately twice that of the O-site ($r_T = 0.291\ R$ vs $r_O = 0.155\ R$, where R is the radius of the host metal atom).[1] Interestingly, the interstitial solutes choose to take the O-sites rather than the larger T-sites.[1,3] To date, however, this commonly accepted picture remains largely an inference from fitting the X-ray diffraction[4] and internal friction[5] data, rather than a direct observation, as imaging the light solute atoms dissolved in the host metal is highly challenging. This brings up the first question that we would like to resolve in this work; seeing is believing; would it ever be possible to directly observe individual solute atoms, and on top of that, tell apart which specific interstitial sites they occupy in bcc interstitial solid solutions?

The next question is about the O-site preference, which has been rationalized in the literature as follows.[1,3] The carbon, oxygen, and nitrogen solutes are significantly larger in size than the open volume available at either the O-site or the T-site, such that a significant lattice distortion is incurred in both cases, upon the introduction of a solute atom. The T-interstice has four nearest-neighbor host atoms, and the displacement of these metal atoms would entail higher strain energy than that for the O-site, which has only two nearest-neighbor metal atoms. As the latter incurs a lower penalty in elastic strain energy,[3] the interstitial solutes would rather squeeze into the O-sites even though the T-sites are larger. This naturally invites a second question, which is another long-standing issue we would like to address in this work, namely, would the octahedral occupancy persist, or would the solutes switch to the larger T-sites, when the solute concentration increases to much higher levels? The latter seems plausible, in the following thought experiment. A bcc crystal has an atomic packing fraction of 68%[3] and hence potentially ample excess volume to accommodate a sizable concentration of solutes. One can envision that at such high concentrations the solutes would eventually feel the presence of one another, as the positions of neighboring metal atoms would become influenced by other solutes in nearby interstices and the lattice expansion accommodating these interstitials. The constraints on both the O-site and T-site would

C. Liu, B. Zhang, J. Ding, E. Ma
Center for Alloy Innovation and Design (CAID)
State Key Laboratory for Mechanical Behavior of Materials
Xi'an Jiaotong University
Xi'an 710049, China
E-mail: maen@xjtu.edu.cn

J. Cui, Z. Cheng, R. Yu
MOE Key Laboratory of Advanced Materials
School of Materials Science and Engineering
Tsinghua University
Beijing 100084, China
E-mail: ryu@tsinghua.edu.cn

S. Zhang
Max-Planck-Institut für Eisenforschung
40237 Düsseldorf, Germany

The ORCID identification number(s) for the author(s) of this article can be found under https://doi.org/10.1002/adma.202209941.

DOI: 10.1002/adma.202209941

then become similar, both involving a similar number of surrounding metal atoms. As the advantage of the O-site occupation diminishes, eventually the larger excess volume available at the T-sites may become the deciding factor to make them the more favored choice.

This study is designed to resolve the two challenging issues raised above. To this end, we examine a model bcc solution with a rather high oxygen content, following a two-pronged strategy. First, on the side of selecting the bcc solution, we take advantage of the recently developed "massive interstitial medium-entropy alloys (MEA),"[6] an example of which being the O-12 alloy[6] with an overall sample composition of $(TiNbZr)_{86}O_{12}C_1N_1$ (at%). This MEA is based on equiatomic bcc TiZrNb alloy as the matrix, with large amounts (sample average ≈12 at%) of oxygen dissolved as interstitials. Different from conventional solutions, the O-12 alloy is composed of multiple principal elements,[7,8] with larger lattice distortion as well as a larger lattice parameter. The overall oxygen content dissolvable in the alloy, before the precipitation of intermetallic second phases,[2] is consequently high. This elevated oxygen concentration not only makes it easier to locate the solutes in atomic-scale microscopy experiments, but also enters a regime well suited for us to probe if a high concentration of interstitial solutes would indeed push them toward the larger and more populous T-sites, in lieu of the O-sites at low oxygen concentrations.

Second, on the side of the imaging capability, we resort to the state-of-the-art electron ptychography, a recently emerging technique powerful for observing light element atoms in a metal matrix.[9,10] This computational imaging method combines scanning transmission electron microscopy (STEM) and coherent diffractive imaging, offering a phase contrast imaging route[10] with advantages well beyond other alternatives that also make use of aberration-corrected STEM. Specifically, while high-angle annular dark-field (HAADF)-STEM is generally adequate in providing interpretable *Z*-contrast images,[11] it often falls short in simultaneously imaging heavy (high-*Z*) metal atoms and lightweight (low-*Z*) atoms.[12] This is because the scattering strength of the light elements is too low for them to be detected, in the presence of other coexisting species with markedly higher atomic numbers. Annular bright-field (ABF)-STEM[13] is more amenable to observing light elements, but failed to produce evidence of oxygen in O-sites in a bcc β-Ti alloy[14] even with a series of through-focus experiments. The integrated differential phase contrast (iDPC) technique takes advantage of the phase contrast imaging,[12] but its spatial resolution is inadequate. Moreover, the oxygen atoms, if successfully observed, could be subjected to doubts as to if they are artifacts arising from oxidation on the surface of the very thin transmission electron microscopy (TEM) specimen. All these challenges can be resolved using multislice electron ptychography, which not only provides superhigh resolution down to deep-sub-angstrom, but can also simultaneously image heavy and light atoms as the phase contrast scales with the atomic number with great linearity.[9] Furthermore, by dissecting a TEM specimen into multiple thin slices, this technique also adds another dimension to the 3D phase distribution information—depth resolution, which will be exploited to exclude possibly contaminated surface layers (to be discussed later). In addition, by using an adaptive propagator (APP) to describe the electron propagation between adjacent slices, the misorientation in the sample can be eliminated without any extra postprocessing.[10] The high misorientation tolerance of the APP-multislice ptychography is especially suited for imaging medium-/high-entropy alloys with large lattice distortion and atomic-scale chemical fluctuations. Taking all these attributes together, the ptychographic phase retrieval affords the highest sensitivity and credence in pinpointing the locations of oxygen in our O-12 solution.

2. Results and Discussion

The details about the preparation of the O-12 alloy samples are presented in the Experimental Section (Supporting Information). Figure S1 (Supporting Information) presents HAADF-STEM images, with the corresponding fast Fourier transform (FFT) patterns in the inset. There is no indication of any other phase beside the bcc structure, i.e., all the oxygen solutes have been dissolved into the host without precipitating out a second phase. The atomic-resolution energy-dispersive X-ray spectroscopy (EDS) mapping (Figure S2, Supporting Information) of the four constituent species shows compositional variations similar to those previously observed in some high-entropy alloys[15–17] (especially if chemical short-range order is present[16]). In addition to the electron microscopy investigation, we performed atom probe tomography (APT) analysis to examine the 3D element distribution in the O-12 alloy (**Figure 1**). The contents of carbon and nitrogen are fairly low, with a sample average of <1 at% in the alloy. The carbon and nitrogen concentrations are even lower in the grain interior (each averaging to <0.4 at%; Figure S3, Supporting Information), while segregating to some degree at the grain boundaries.[6] The frequency distribution analysis (Figure 1c) suggests a near-random distribution of Ti, Zr, Nb, and O within the grain, with Pearson coefficients (μ) close to zero. However, upon careful inspection, Nb appears to exhibit a larger μ, suggesting a lower degree of randomness. A hint of inhomogeneous Nb distribution is also observable in Figure 1b, revealing nanoscale Nb concentration fluctuations throughout the APT dataset.

To gauge the self-correlation and cross-correlation of the species, we performed pair-correlation analysis and monitored the distribution of constituent atoms at distance *r* surrounding Nb atoms (Figure 1d). The positive (or negative) correlation is reflected by an increasing (or decreasing) concentration of the specific element in the immediate vicinity of Nb atoms. Figure 1d shows enriched Nb, along with depleted Ti/Zr/O, when approaching Nb. This suggests that at the nearest neighbor's length Nb favors Nb, while disfavoring Ti, Zr, and O. This tendency of preference/avoidance is also manifested in the 1D profile (Figure 1e); from location to location on the scale of around 1 nm, the distribution of Nb appears to be wavy. This concentration undulation is not merely statistical fluctuation, because it is found to negatively correlate with that in the oxygen profile and also negatively with that of Ti/Zr, as seen in Figure 1e. The tendency toward Ti/Zr preference leaving behind Nb has been found earlier[18] for the TiZrNb alloy, and can be partly attributed to the different degrees of chemical affinity between these species; Ti prefers Zr as nearest neighbors and

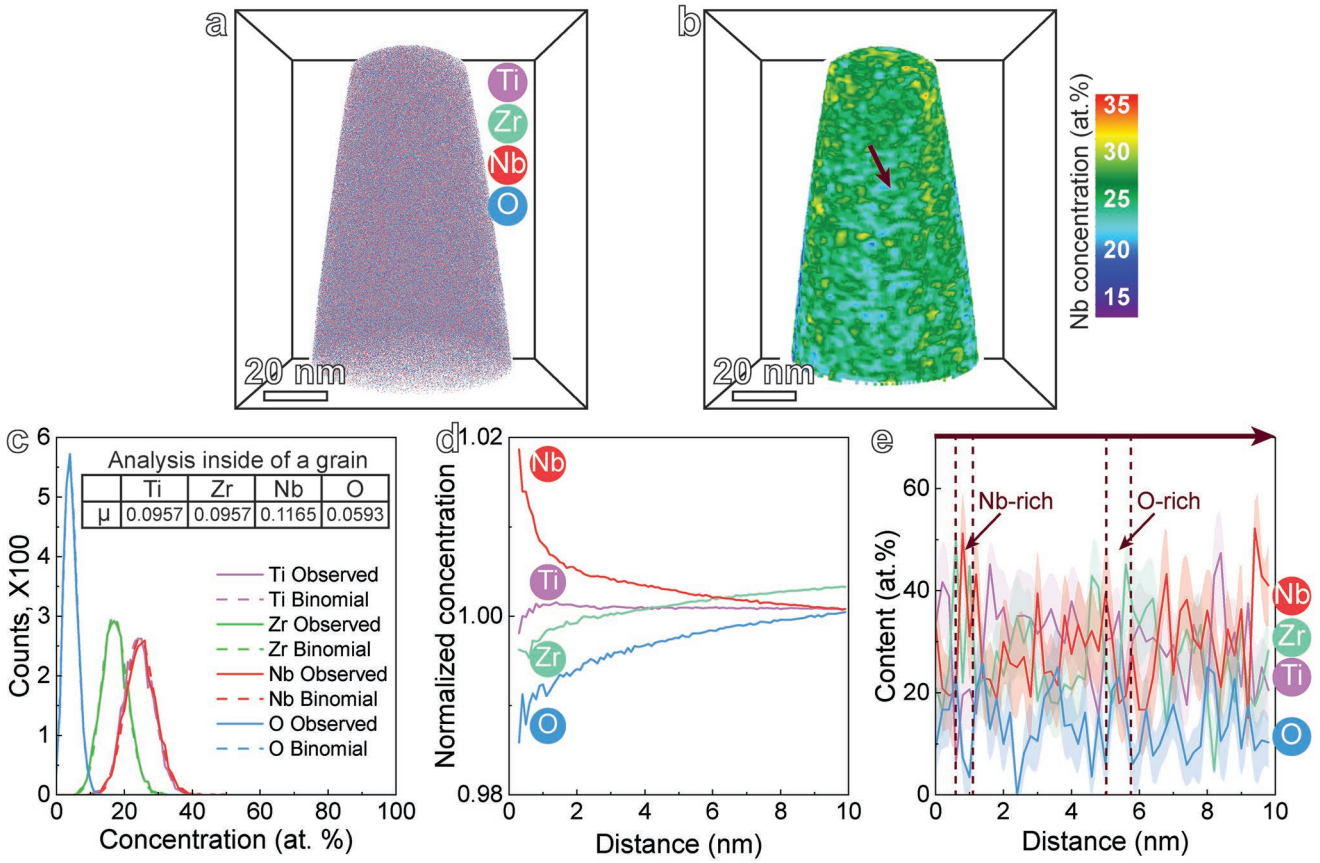

Figure 1. Atom probe tomography (APT) analysis of the O-12 alloy. a) 3D reconstruction of the APT dataset. b) 3D reconstruction map showing nanoscale variations of Nb concentration in the sample. c) Frequency distribution analysis inside of the grain, indicating near-random distribution of the four constituent elements, with Pearson coefficients (μ) close to zero. Nb has a larger μ than the other elements, suggesting a lower degree of randomness. d) Pair-correlation analysis of the species in the APT sample, performed by measuring the concentrations of the constituent elements at distance r from Nb atoms. Nb appears to favor Nb as nearest neighbors, while avoiding Ti, Zr, and O. e) 1D profile measured along the arrow indicated in (b) (see the "Experimental Section" in the Supporting Information). The profile shows correlated compositional undulation on the scale of around 1 nm. Nb-enriched locations correlate with oxygen-depleted ones (and oxygen-enriched corresponding to Nb-depleted), as marked with dashed lines.

both of them prefer intimate bonding with oxygen,[13] rendering local environments enriched in oxygen with respect to the alloy average. The neighboring region is then expected to be enriched in Nb but depleted in the other three elements. This explains the alternating (up and down on the length scale of 1 nm) pattern observed in Figure 1b,e. As a result of this composition undulation exacerbated by local chemical short order, in our O-12 sample, the oxygen concentration varies from one location to another and in some local nanometer regions reach levels clearly above the sample average; see Figure 1e. This expanded composition possibility, due to chemical inhomogeneity on top of the already-high average oxygen concentration in the alloy, increases the opportunities for us to make observations of interstitial site selection at markedly elevated oxygen concentrations.

We now move on to the microscopy experiments (see schematic in **Figure 2**a for the multislice ptychography with an adaptive propagator), beginning with imaging along the [001] zone axis (the crystal structure model, showing the locations of the T- and O-interstices, is given in Figure 2b). In the ptychography phase image of Figure 2c, the metal atoms are seen to take the bcc lattice, while additional interstitial atoms are seen at the interstices of the bcc lattice; compared to the metal atoms, much weaker intensities are seen for those at interstices, suggesting that they originate from oxygen atoms. This intensity contrast is expected due to the large disparity in the atomic weight between oxygen and the metallic species (Ti, Nb, and Zr). To demonstrate that these dimmer columns indeed arise from interstitial atoms rather than background noise, we plot, in Figure 2e,f an intensity profile along the interstices in the bcc lattice; the interstitial site shows significantly higher intensity above the background. Comparing the above experimental observation with the structure model in Figure 2b viewed along the same zone axis, we have the first indication that some oxygen interstitials are present at the T-sites; the high spatial resolution of ptychography enabled us to see dim spots that are close to, and branch out from, the metal atoms, at locations expected from tetrahedral interstitials (compare with insets in Figure 2c). However, this identification is not without ambiguities. In this viewing direction, the easiest interstitial atom to see, i.e., the one with a relatively high intensity and large distance from the metal atoms, is located at the center of the space enclosed by four metal atoms. But along this column T-sites and O-sites sit on top of each other (labeled T&O in the

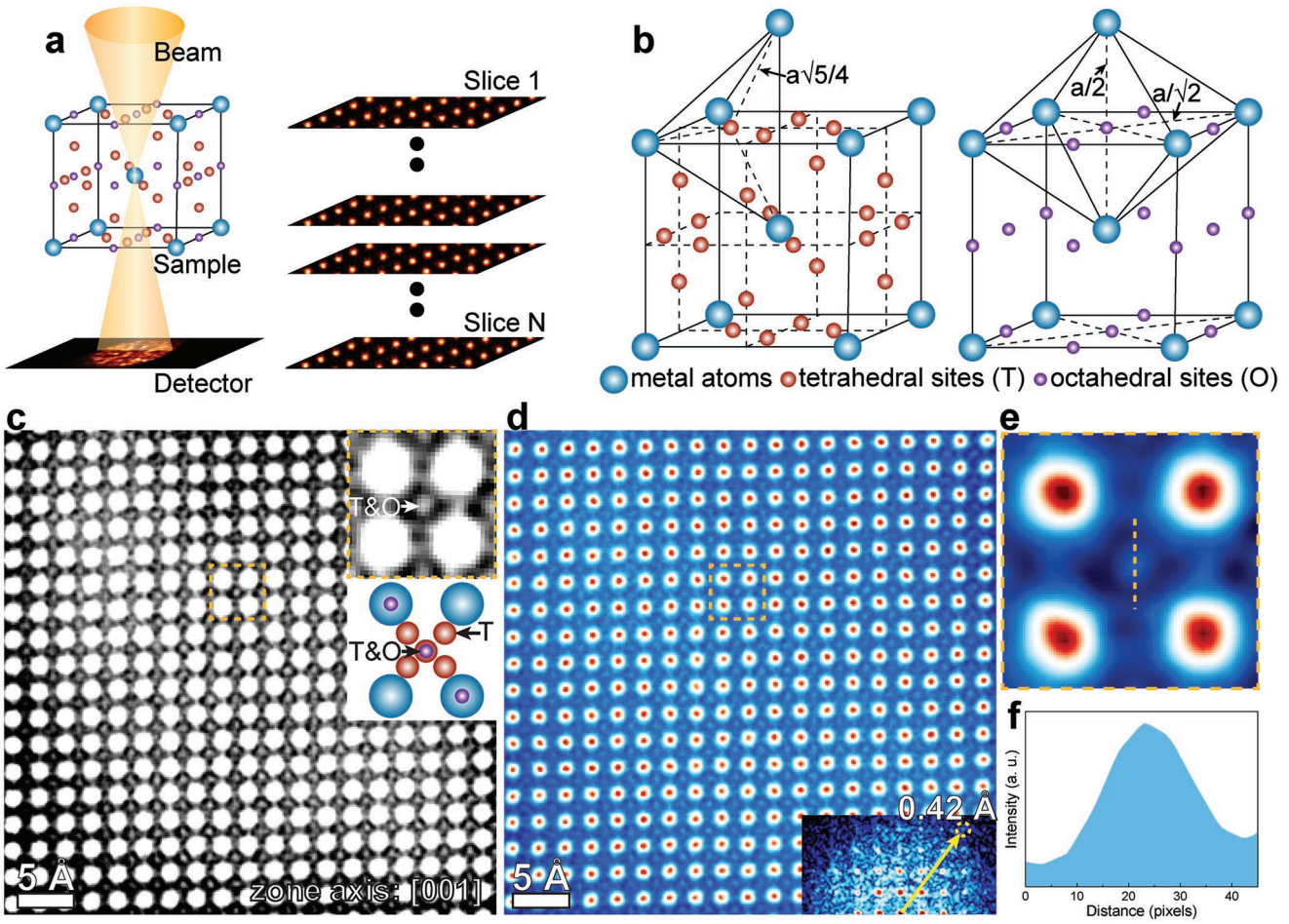

Figure 2. Multislice ptychography characterization of the O-12 alloy, enabling direct observation of the oxygen interstitials in the bcc lattice. a) Schematic of the multislice ptychography with an adaptive propagator (APP), the scanning diffraction patterns were obtained using a pixel array detector equipped in an aberration-corrected electron microscope. b) Crystal structure model of the tetrahedral (T) and octahedral (O) interstices in a bcc lattice. c) Phase image of the O-12 alloy observed along the [001] zone axis. The insets show a close-up image of the yellow rectangle region in (c) and a structural model of the bcc lattice with T-sites and O-sites interstitials projected along the [001] zone axis. d) Phase image corresponding to (c); the image was colored for better illustration. The inset in (d) shows the corresponding Fourier transformation pattern, demonstrating a spatial resolution of 0.42 Å. e) Close-up image of the yellow rectangle region in (d). f) Profile of phase intensity along the yellow dashed line in (e).

insets in Figure 2c). The intensity observed there could then be from oxygen in either the T-sites or O-sites, or both. Therefore, to avoid this superimposition we need to move to the [011] and/or [111] zone axis to better distinguish the T-sites and O-sites.

We now emphasize a critical niche of our multislice technique, i.e., we are able to avoid likely artifacts and biased analysis caused by surface oxidation, by using only the slices obtained near the center of the TEM sample (slices numbered from 4 to 12 in our case, to extract data presented in Figure 2) for analyzing oxygen interstitials. The depth sectioning of the O-12 sample by APP multislice electron ptychography is shown in Figure S4 (Supporting Information). The slices measured at the top (slice 1) and bottom (slice 15) of the sample reveal significantly higher amounts of oxygen interstitials than those (slice 8) at the center. This result suggests that the oxidation of the sample surface could interfere with the observations and the associated data should be treated with a grain of salt. We therefore decided to leave out those questionable slices close to the top and bottom surfaces.

By moving to [011] and [111] zone axes, we were able to obtain unequivocal evidence for oxygen interstitials occupying T-sites in the bcc interstitial solid solution. **Figure 3**a,b presents the APP electron ptychography observation of the O-12 alloy along the [011] zone axis. The oxygen interstitials are clearly observed in the interstices of the bcc lattice, but now the T- and O-sites can be unambiguously distinguished under this zone axis. To demonstrate this, the close-up view of the phase image and the crystal structure model are compared in Figure 3b. In this particular region, the oxygen interstitials are located at T-sites only, with the O-sites left unoccupied. To visualize the spatial distribution/density of oxygen interstitials in the bcc lattice, we then plotted 2D maps of normalized intensity of the T- and O-sites (Figure 3c,d). We observe that the tetrahedral interstitials tend to agglomerate in regions where there are also aggregated octahedral interstitials (Figure 3c,d). This suggests that these are oxygen-enriched regions, where the oxygen interstitial population is higher than the surroundings. The maps suggest ≈1 nm sized oxygen-enriched regions alternating with those

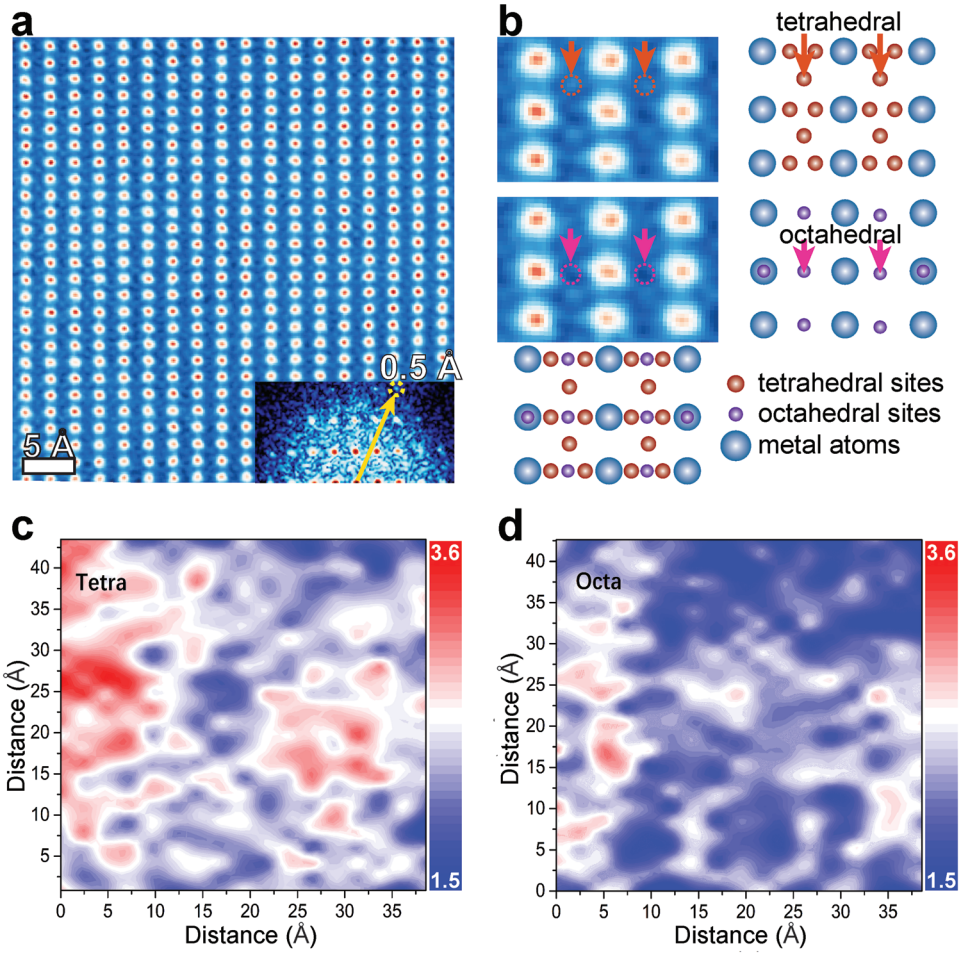

Figure 3. Multislice ptychography imaging of the O-12 alloy along the [110] zone axis, showing oxygen interstitials occupying the T-sites. a) Observation of the O-12 alloy along the [110] zone axis. The inset in (a) shows the corresponding Fourier transformation pattern, indicating a spatial resolution of 0.5 Å. b) Close-up image of (a), compared with structural models of bcc lattice containing T-site and O-site interstitials projected along the [110] zone axis. The oxygen interstitials occupy the T-sites, rather than the O-sites, in this region. c,d) Contour map of normalized intensity reflecting the spatial distribution of T-sites and O-sites in (a).

containing lower concentrations of oxygen. This observation of chemical inhomogeneity, on the scale of 1 nm, agrees with the APT analysis (Figure 1). As discussed earlier, this chemical inhomogeneity is partly originated from the stronger affinity of oxygen with Ti/Zr relative to Nb,[18] rendering local regions with oxygen concentration above the already-high sample average. The presence of nanometer-sized oxygen complexes, composed of enriched Ti and Zr together with interstitial O believed to occupy both the O sites and T sites, was reported earlier in an oxygen (2 at%) doped TiZrNbHf alloy.[13] Our results above, on the other hand, explicate that the tendency toward the unusual T-site preference is causally correlated with the elevated oxygen concentrations.

Similar observations and conclusions have been made, when observing the alloy along the [111] zone axis. The results in this viewing direction are shown in **Figure 4**. Again, intensities of interstitial solutes show up mainly at the T-sites. Considering that the probabilities for oxygen to take the T-site and O-site are at least similar (see also Figure 3), and that the bcc unit cell has more T-sites than O-sites, the total oxygen atoms taking the T-sites would outnumber those taking the O-sites in this bcc structure. This affirms our claim that, dramatically different from the traditional belief of interstitials occupying O-sites only in a bcc lattice,[1,3] at high oxygen concentrations the T-site interstitials become dominant.

The trend toward T-sites at elevated solute concentrations can be rationalized as follows. When an oxygen interstitial is introduced into the T-site of the parent Ti–Zr–Nb alloy, it would spontaneously jump to the nearest O-site after structural relaxation (see schematic in Figure S5 in the Supporting Information). As illustrated in Figure S6 (Supporting Information), in a bcc metal with dilute interstitials, each interstitial entering the O-site would displace only the two closest metal atoms from their original sites, incurring less strain energy than that required for pushing apart four metal atoms, as in the T-site case. This strain consideration as a key component of the overall free energy underlies the prevailing belief that interstitials take residence in the O-sites of a bcc metal.[1,3] However, at high oxygen concentrations, additional constraints come into play on the metal atoms that need to be displaced when

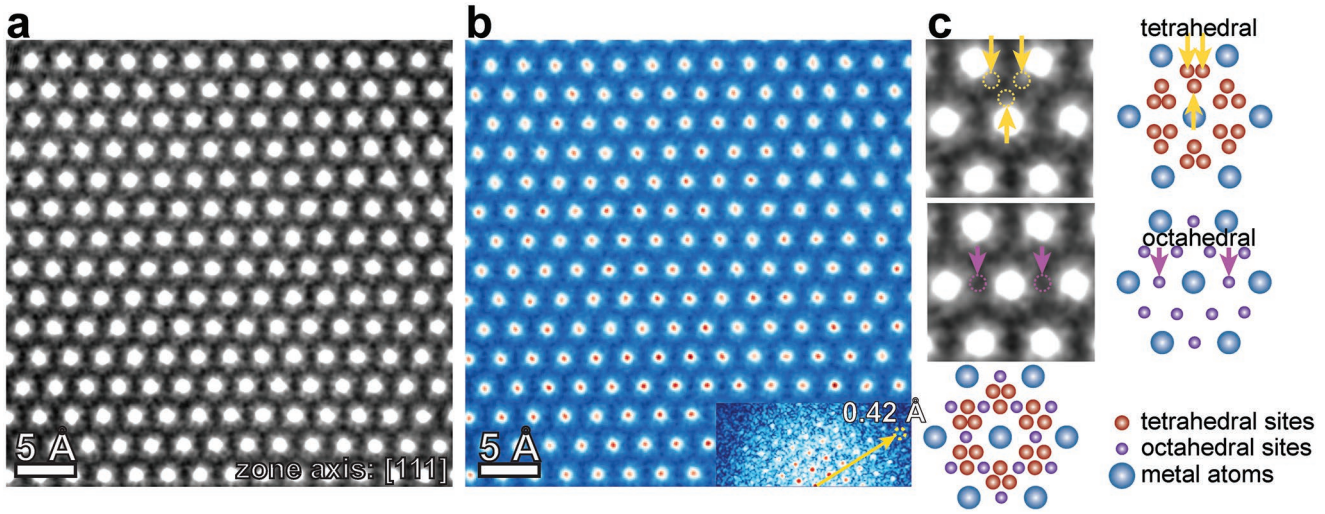

Figure 4. Multislice ptychography observation of the O-12 alloy along the [111] zone axis. a,b) Phase images of the O-12 alloy. The inset in (b) shows the corresponding Fourier transformation pattern, indicating a spatial resolution of 0.42 Å. c) Close-up image of (a), and structural models of bcc lattice projected along the [111] zone axis. The oxygen interstitials are preferentially located in the T-sites, corroborating the observation along the [110] zone axis (Figure 3).

the solute enters the O-site. As schematically depicted in Figure S6 (Supporting Information), at high interstitial concentrations, there will be interstitials in the immediate surroundings, which impose constraints on the metal atoms to be displaced. As a result, the strain energy required for an octahedral interstitial to displace the neighboring metal atoms is significantly increased, and with more interstitials in the neighborhood eventually becomes comparably high with that required for the tetrahedral interstitial. With this strain advantage taken away, the O sites is expected to become disfavored when compared with the more spacious T sites. A transition from O-sites to the larger T-sites would be even more likely as the oxygen distribution is inhomogeneous, which inevitably results in some local regions more crowded with oxygen interstitials.

3. Conclusions

We have answered the two questions raised at the outset of this work. First, the state-of-the-art adaptive propagator multislice electron ptychography allowed us to not only directly observe oxygen solute atoms in the bcc interstices, but also distinguish tetrahedral versus octahedral sites thanks to the high spatial resolution of the technique. The multislice capability enabled depth profiling to ensure that the information is from the sample interior without possible complications from TEM specimen surfaces. Second, in addition to the normally accepted interstitial occupancy of octahedral sites in bcc structure, we provide clear evidence of oxygen in unusual tetrahedral sites, which in fact becomes the majority scenario in regions with elevated solute concentrations. This change in site preference is explained by considering the strain energy cost incurred to accommodate the octahedral oxygen interstitials, in the presence of additional oxygen solutes nearby. The direct evidence provided by our atomic-level observations is expected to put to rest some of the existing myths regarding bcc interstitial solid solutions. The expanded realm to cover tetrahedral interstices has a profound impact to the composition design and strengthening possibilities of solid solutions. For example, our findings could serve as a stepping stone for exploiting synergistic benefits combining multi-principal-element substitutional (the so-called medium-/high-entropy alloys) and "massive" interstitial (high and undulating solute concentrations as described above) solid-solution hardening, which holds promise for record high strength/hardness for solid-solution alloys.[6]

Supporting Information

Supporting Information is available from the Wiley Online Library or from the author.

Acknowledgements

C.L., J.C., and Z.C. contributed equally to this work. The support from National Natural Science Foundation of China (Grant Nos. 52231001 and 51788104) was gratefully acknowledged. C.L. acknowledges support from National Natural Science Fund for Excellent Young Scientists Fund Program (Overseas). J.D. acknowledges support from National Natural Science Foundation of China (Grant No. 12004294), National Youth Talents Program and the HPC platform of Xi'an Jiaotong University. E.M., C.L., and J.D. are indebted to Xi'an Jiaotong University for hosting their work at the Center for Alloy Innovation and Design (CAID).

Conflict of Interest

The authors declare no conflict of interest.

Data Availability Statement

The data that support the findings of this study are available from the corresponding author upon reasonable request.

Keywords

body-centered-cubic metals, electron ptychography, high-entropy alloys, interstitials, medium-entropy alloys

Received: October 27, 2022
Revised: November 28, 2022
Published online: February 17, 2023

[1] R. E. Smallman, R. J. Bishop, *Modern Physical Metallurgy and Materials Engineering*, 6th ed., Elsevier, Oxford, UK **1999**.
[2] F. C. Campbell, *Elements of Metallurgy and Engineering Alloys*, ASM International, Materials Park, OH, USA **2008**.
[3] G. Gottstein, *Physical Foundations of Materials Science*, Springer, New York **2013**.
[4] C. Garcia-Mateo, J. A. Jimenez, H. W. Yen, M. K. Miller, L. Morales-Rivas, M. Kuntz, S. P. Ringer, J. R. Yang, F. G. Caballero, *Acta Mater.* **2015**, *91*, 162.
[5] W. S. Choi, J. Lee, B. C. De Cooman, *Mater. Sci. Eng., A* **2015**, *639*, 439.
[6] C. Liu, W. Lu, W. Xia, C. Du, Z. Rao, J. P. Best, S. Brinckmann, J. Lu, B. Gault, G. Dehm, G. Wu, Z. Li, D. Raabe, *Nat. Commun.* **2022**, *13*, 1102.
[7] J. W. Yeh, S. K. Chen, S. J. Lin, J. Y. Gan, T. S. Chin, T. T. Shun, C. H. Tsau, S. Y. Chang, *Adv. Eng. Mater.* **2004**, *6*, 299.
[8] B. Cantor, I. T. H. Chang, P. Knight, A. J. B. Vincent, *Mater. Sci. Eng., A* **2004**, *375–377*, 213.
[9] Z. Chen, Y. Jiang, Y.-T. Shao, M. E. Holtz, M. Odstrčil, M. Guizar-Sicairos, I. Hanke, S. Ganschow, D. G. Schlom, D. A. Muller, *Science* **2021**, *372*, 826.
[10] H. Sha, J. Cui, R. Yu, *Sci. Adv.* **2022**, *8*, eabn2275.
[11] H. Sawada, T. Sasaki, F. Hosokawa, K. Suenaga, *Phys. Rev. Lett.* **2015**, *114*, 166102.
[12] S. de Graaf, J. Momand, C. Mitterbauer, S. Lazar, B. J. Kooi, *Sci. Adv.* **2020**, *6*, eaay4312.
[13] Z. Lei, X. Liu, Y. Wu, H. Wang, S. Jiang, S. Wang, X. Hui, Y. Wu, B. Gault, P. Kontis, D. Raabe, L. Gu, Q. Zhang, H. Chen, H. Wang, J. Liu, K. An, Q. Zeng, T.-G. Nieh, Z. Lu, *Nature* **2018**, *563*, 546.
[14] X. Fu, X. Wang, B. Zhao, Q. Zhang, S. Sun, J. Wang, W. Zhang, L. Gu, Y. Zhang, W. Zhang, W. Wen, Z. Zhang, L. Chen, Q. Yu, E. Ma, *Nat. Mater.* **2022**, *21*, 290.
[15] Q. Ding, Y. Zhang, X. Chen, X. Fu, D. Chen, S. Chen, L. Gu, F. Wei, H. Bei, Y. Gao, M. Wen, J. Li, Z. Zhang, T. Zhu, R. O. Ritchie, Q. Yu, *Nature* **2019**, *574*, 223.
[16] X. Chen, Q. Wang, Z. Cheng, M. Zhu, H. Zhou, P. Jiang, L. Zhou, Q. Xue, F. Yuan, J. Zhu, X. Wu, E. Ma, *Nature* **2021**, *592*, 712.
[17] Y. Bu, Y. Wu, Z. Lei, X. Yuan, H. Wu, X. Feng, J. Liu, J. Ding, Y. Lu, H. Wang, Z. Lu, W. Yang, *Mater. Today* **2021**, *46*, 28.
[18] K. Xun, B. Zhang, Q. Wang, Z. Zhang, J. Ding, E. Ma, *J. Mater. Sci. Technol.* **2023**, *135*, 221.